



Lateral confinement enhanced membrane laser on Si with a buried-ridge-waveguide structure

NAOKI TAKAHASHI,^{1,*} WEICHENG FANG,¹ YOSHITAKA OHISO,¹ TOMOHIRO AMEMIYA,^{1,2} AND NOBUHIKO NISHIYAMA^{1,2}

¹Department of Electrical and Electronic Engineering, Tokyo Institute of Technology, Tokyo 152-8552, Japan

²Institute of Innovative Research (IIR), Tokyo Institute of Technology, Tokyo 152-8552, Japan

*Corresponding author: takahashi.n.av@m.titech.ac.jp

Received 21 July 2021; revised 18 September 2021; accepted 19 September 2021; posted 20 September 2021 (Doc. ID 438329); published 18 October 2021

The energy consumption of light sources must be reduced to realize on-chip optical interconnects. This study proposes a buried-ridge-waveguide (BRW) structure to enhance the lateral optical confinement. An increase in the lateral optical confinement induces the reduction in the threshold current, and it also provides a differential resistance due to a reduction in the distance between the electrode and active region. The stripe width and ridge height are designed considering the internal loss and differential resistance. A comparison between the BRW and conventional flat structures demonstrates a 20% and 35% reduction in the threshold current and differential resistance, respectively. © 2021 Optical Society of America

<https://doi.org/10.1364/JOSAB.438329>

1. INTRODUCTION

The performance of large-scale integrated (LSI) circuits has been improved due to the scaling law [1]. However, the scaling of transistors also causes wiring delays and Joule heating in the global electrical wiring layer of the LSI [2,3]. These problems can be solved by replacing the electrical global wiring with optical wiring [4–6]. The realization of on-chip optical interconnects requires a light source with ultralow power consumption and a data transmission energy cost of less than 10 fJ/bit [7]. The light source is also required to emit sufficient light to be detected by the low-power consumption receiver and which can be integrated easily with passive devices in an in-plane platform. Vertical-cavity surface-emitting lasers (VCSELs) [8–11], microdisk lasers [12–15], and photonic crystal lasers [16–21] have been reported as light sources for low-power-consumption operation. However, it is difficult for these lasers to produce sufficient light output while maintaining the ease of integration with other devices.

In order to meet these requirements, this study proposes a membrane distributed-reflector (DR) laser as a light source [22–26]. Several groups have also fabricated lasers and other devices using the membrane structure [27,28]. A dielectric material such as SiO₂ or air can be used instead of a semiconductor for the upper and lower claddings to obtain large refractive index difference in the membrane laser. This large refractive index difference induces an increase in the optical confinement factor by approximately 3 times when compared to the conventional structure, leading to a reduction in the threshold current as well as a higher modulation efficiency. Additionally,

bonding technology enables in-plane integration with other passive devices on a Si substrate. Thus, the membrane laser is a promising light source for on-chip optical interconnects.

Low threshold current and high-efficiency operation of membrane DR lasers with an energy cost of 93 fJ/bit have been demonstrated [26]. However, the energy cost must be further reduced to realize practical on-chip optical interconnects [7]. The membrane laser has been reported by several groups, and strong optical confinement was achieved in the vertical direction. However, for lateral injection type membrane lasers, confinement in the lateral direction was weak due to small refractive index difference between active region and side cladding region [29]. This paper proposes a structure that improves the lateral optical confinement and presents the results of the reduction of the threshold current and differential resistance.

2. DEVICE STRUCTURE

The membrane laser consists of a 1.55 μm band GaInAsP-based multiple quantum well (MQW) that is vertically sandwiched by InP, with a total thickness of 270 nm; it also has a lateral $p-i-n$ junction with InP side cladding layers. Consequently, an insulating material with a low refractive index can be used for the top and bottom cladding layers, which enables the realization of strong vertical optical confinement. However, the optical confinement is not strong in the lateral direction because of the small refractive index difference between the GaInAsP active layer and the InP side cladding layers as shown in Fig. 1(a).

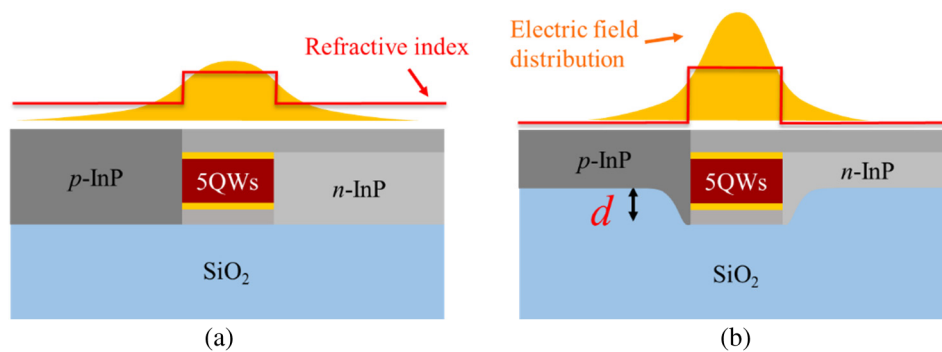


Fig. 1. Cross-sectional view of membrane laser with (a) the conventional flat structure and (b) the BRW structure.

Therefore, this study introduces a buried-ridge-waveguide (BRW) structure to enhance the lateral optical confinement as shown in Fig. 1(b).

The introduction of a height difference between the GaInAsP active layer and the InP side cladding layer enables the realization of a relatively large refractive index difference, which results in stronger optical confinement in the lateral direction when compared to that of the conventional structure. Figure 2(a) shows the dependence of the optical confinement factor on the calculated stripe width (active layer width) of the active region with ridge height d as a parameter. The other calculation parameters are listed in Table 1. The optical confinement is enhanced by the increase in the ridge height d and the stripe width. In this study, the stripe width is set to $1.8 \mu\text{m}$ for the fabrication. Figures 2(b) and 2(c) show the mode distribution of the conventional structure and the BRW structure ($d = 50 \text{ nm}$) at a stripe width of $W_s = 1.8 \mu\text{m}$. It is observed that the mode is confined better in the lateral direction for the BRW structure, and the optical confinement in the active layer is increased when compared to that of the conventional structure.

Furthermore, the increase in the lateral optical confinement due to the adoption of the BRW structure also contributes to the reduction of the differential resistance of the membrane laser. The electrodes deposited on the side cladding layer must be sufficiently separated from the active layer to avoid overlap with the optical mode. In a conventional flat structure, a high differential resistance was observed due to the long distance

Table 1. Parameters in the Mode Calculation

Refractive index of InP	3.17
Refractive index of GaInAsP (well)	3.54
Refractive index of GaInAsP (barrier)	3.35
Thickness of GaInAsP active layers [nm]	120
Total thickness of III-V layer [nm]	270

between the electrode and the active region due to weak optical confinement in the lateral direction. However, the enhancement of the optical confinement in the lateral direction in the BRW structure enables the electrode deposited in the side cladding to be brought closer to the active layer when compared to the conventional structure, and the differential resistance can be reduced accordingly.

Figure 3(a) shows the calculated internal loss α_i as a function of the ridge height d and the distance D between the edges of the p -electrode and the active region. The white lines in the figures are borderline if a 5% increase in the internal loss is allowed when compared to the internal loss when the electrode is set to sufficiently far. As observed, the minimum distance D_{min} can be decreased by increasing the ridge height d ($D_{\text{min}} = 1.6 \mu\text{m}$ at $d = 0$, whereas $D_{\text{min}} = 0.7 \mu\text{m}$ at $d > 50 \text{ nm}$). Figure 3(b) shows the calculated resistance R when the ridge height d and distance D are changed. In this calculation, it is assumed that the resistance in the p -InP side cladding layer is dominant. The increase in the ridge height d causes thinning of the current pass and an increase in the resistance per unit length. Therefore, the

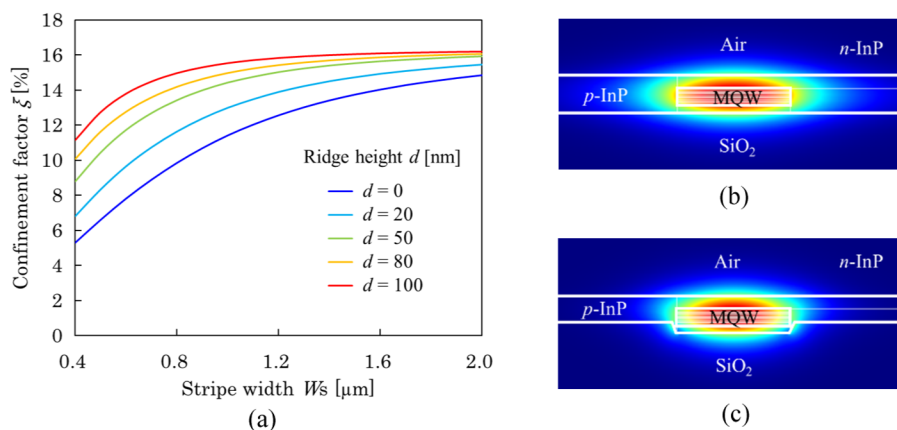


Fig. 2. (a) Calculated stripe width dependence of the optical confinement factor for various ridge height d . Calculated optical intensity distribution of (b) the conventional flat structure and (c) the BRW structure ($d = 50 \text{ nm}$) at a stripe width of $1.8 \mu\text{m}$.

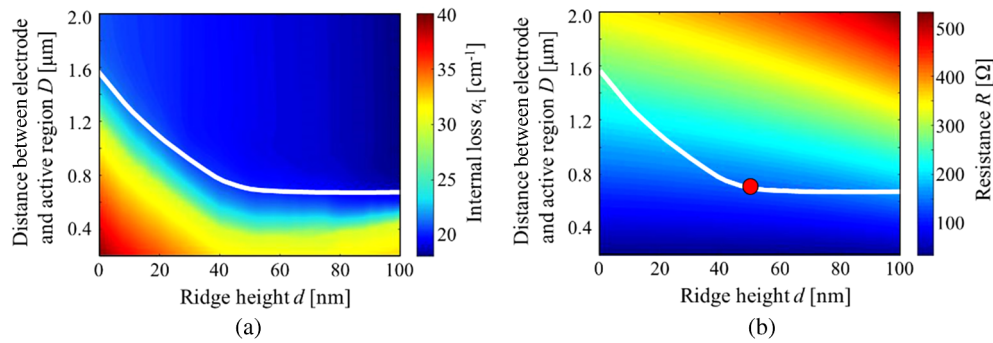


Fig. 3. (a) Calculated internal loss α_i with various ridge height d and distance D between the p -electrode and the active region. (b) Calculated resistance R with various ridge height d and distance D .

resistance R is the lowest at $d = 50$ nm on the borderline. At this value, a resistance reduction of 40% can be realized when compared to that of the conventional flat structure.

3. DEVICE FABRICATION AND CHARACTERIZATION

The membrane lasers with a BRW structure are fabricated based on the analysis results presented above. The device fabrication process is as follows: a 270 nm thick core layer including strain-compensated GaInAsP five quantum wells (5QWs) sandwiched by InP optical confinement layers are grown on an n -InP substrate by organometallic vapor-phase epitaxy (OMVPE) [Fig. 4(a)]. The active layer is etched [Fig. 4(b)] and buried with n -InP on one side and p -InP on the other side to form a p - i - n junction [Fig. 4(c)] through selective area regrowth. Subsequently, it is bonded upside down on the Si substrate by benzocyclobutene (BCB) bonding [Fig. 4(d)] after depositing a 1 μ m thick SiO₂ layer on the laser wafer. The membrane structure is then obtained by removing the InP substrate [Fig. 4(e)]. Lastly, the metal electrodes are deposited on the contact layer formed on the side cladding InP [Fig. 4(f)].

The BRW structure is formed through selective area regrowth using a SiO₂ mask while forming a buried p - i - n junction [Fig. 4(c)]. The mask width and growth time are tuned to realize the BRW structure with a ridge height of 50 nm, which is designed from the calculation. Figure 5 shows the cross-sectional scanning electron microscope (SEM) image of the selective area regrowth controlled the growth period of the InP by inserting GaInAs marker layers. The growth by OMVPE is performed under the following conditions: V/III ratio of 550, pressure of 76 Torr, and temperature of 600°C. The growth period of the InP and GaInAs aimed at thicknesses of 40 nm and 10 nm is 47 s and 8 s, respectively. Consequently, the desired BRW structure can be obtained by growing n -InP for 2.8 min and p -InP for 4.5 min at a mask width of 125 μ m.

Figures 6(a) and 6(b) show the cross-sectional SEM images of the fabricated membrane Fabry–Perot lasers with the conventional flat structure and the BRW structure, respectively. Figure 7 shows the I - L and I - V characteristics of the fabricated devices with a cavity length of 560 μ m and a stripe width of 1.8 μ m. The electrodes are formed with a distance D of 1.7 μ m (conventional structure) and 0.8 μ m (BRW structure) as determined by the theoretical calculation presented above.

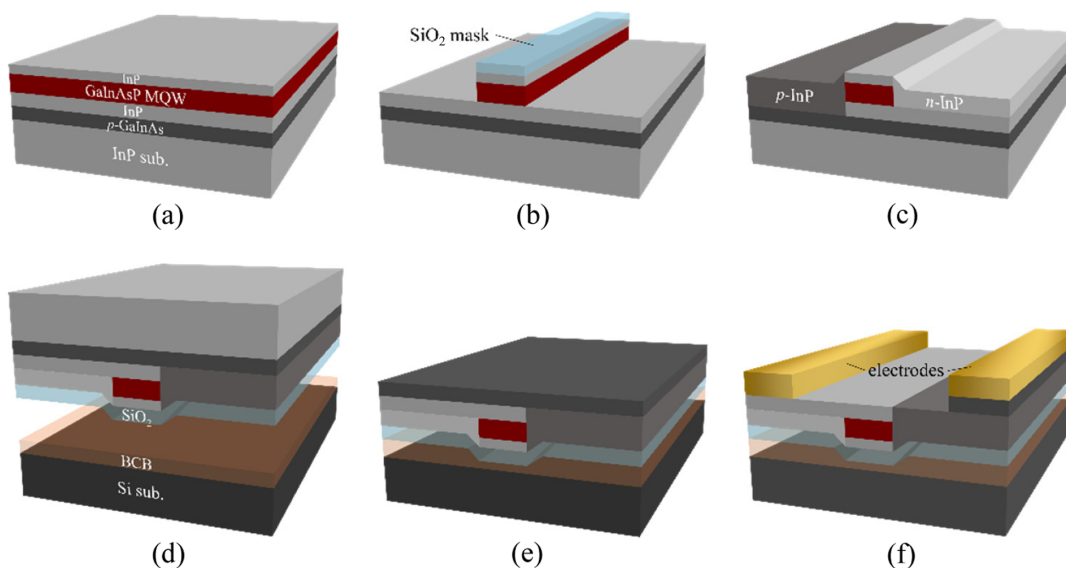


Fig. 4. Fabrication process of the membrane Fabry–Perot laser.

The characterizations are performed under room-temperature continuous-wave (RT-CW) conditions. The typical lasing wavelength was 1560 nm. The threshold current is 12.5 mA for the conventional flat structure and 9.8 mA for the BRW structure (threshold current densities are calculated to be 1.3 and 1.0 kA/cm², respectively). The differential resistance dV/dI for the flat structure and the BRW structure is 48 and 31 Ω , respectively. Figure 8(a) shows the spectrum of the fabricated device with the cavity length of 560 μm and the current of 20 mA. As can be seen, the lasing spectrum is around 1570 nm. Figure 8(b) shows the horizontal component of the far field pattern with the current of 20 mA. From measurement results indicated by solid line, full width at half-maximum (FWHM) for the BRW and flat structure are calculated 38.0° and 27.8°, respectively. These are close to the results of mode calculation

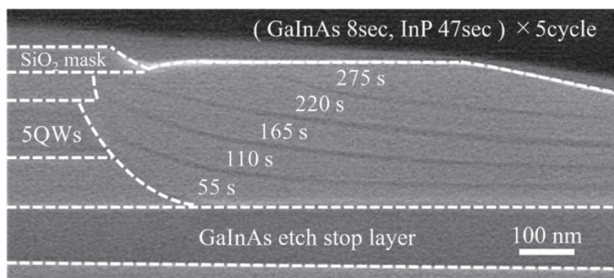


Fig. 5. OMVPE embedding growth pattern of InP with intervals of a GaInAs marker.

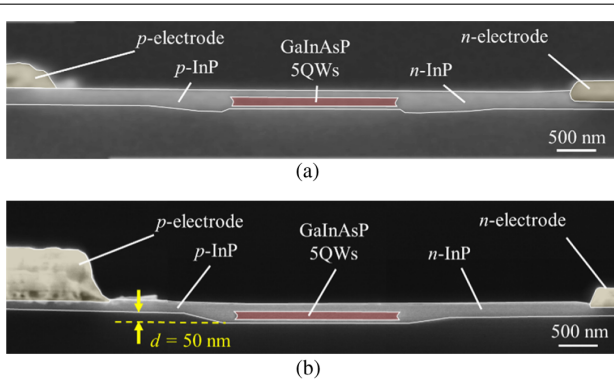


Fig. 6. Cross-sectional SEM images of fabricated membrane Fabry-Perot lasers with (a) the conventional flat structure and (b) the BRW structure. Please note that the SEMs were colored for a clear visual.

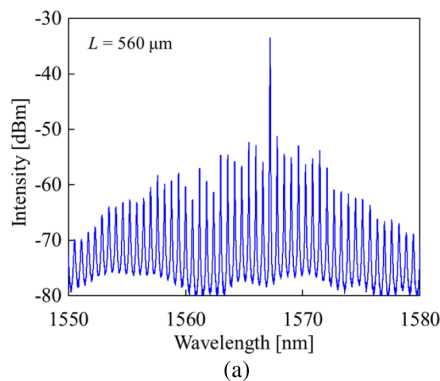


Fig. 8. (a) Spectrum of the fabricated device with cavity length of 560 μm at the bias current of 20 mA. (b) Horizontal component of far-field pattern for the BRW structure and the flat structure.

(38.8° and 28.9°, respectively), and it was confirmed that the expected optical confinement effect was obtained. Figure 9(a) shows the dependence of the threshold current on the cavity length. The BRW structure reduces the threshold current by 20% when compared to the conventional flat structure. This result shows that the BRW structure can effectively reduce the threshold current of the membrane laser by increasing the lateral optical confinement. Figure 9(b) shows the dependence of the differential resistance on the cavity length. It can be observed that the BRW structure reduces the differential resistance by 35% when compared to the conventional flat structure. By introducing the BRW structure, the differential resistance is reduced due to the decrease of distance D from 1.7 to 0.8 μm . The conventional structure with a distance D of 0.8 μm does not lase due to the high optical absorption by the electrode. Assuming that the introduction of the BRW structure into the DFB laser has the same improvement effect as the Fabry-Perot laser, it is expected that energy cost can be reduced by 25% compared with that of the conventional one. In this paper, the thickness of side cladding layers near the active layer changes gradually, the lateral optical confinement can increase slightly more by considering the growth conditions so that the thickness changes sharply.

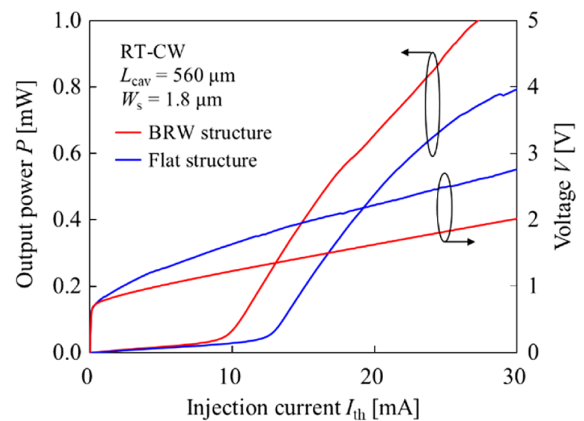
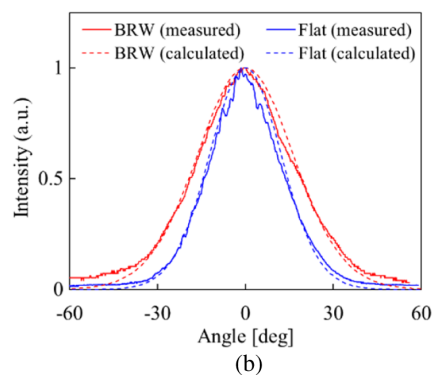


Fig. 7. Current-light output and current-voltage characteristics of membrane Fabry-Perot laser with cavity length of 560 μm and stripe width of 1.8 μm .



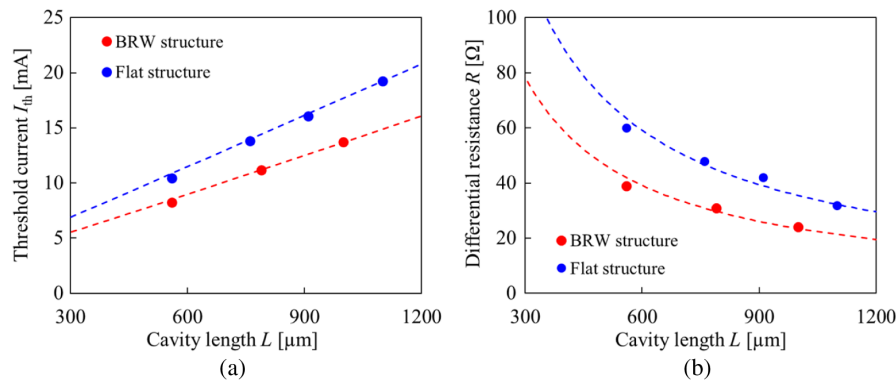


Fig. 9. Comparison of characteristics of BRW structure and conventional structure in (a) cavity length dependence of threshold current I_{th} and (b) cavity length dependence of differential resistance R .

4. CONCLUSION

This study proposes a BRW structure for the low-power-consumption operation of a semiconductor membrane laser.

First, the optical confinement factor and the differential resistance are calculated for various ridge heights d . Based on the correlation between the internal loss and optical confinement, the ridge height d that can reduce the differential resistance most was found to be 50 nm.

A membrane Fabry–Perot laser with a BRW structure was then fabricated and evaluated. By introducing the BRW structure with a ridge height d of 50 nm, a 20% reduction in the threshold current was demonstrated when compared to a conventional flat structure, due to an increase in the lateral optical confinement. Additionally, the reduction in the distance between the electrode and active region induced a 35% reduction in the differential resistance.

These results indicate that the introduction of the BRW structure can effectively reduce the power consumption and realize on-chip optical interconnects.

Funding. Core Research for Evolutional Science and Technology (JPMJCR15N6); Japan Society for the Promotion of Science (19H02193, 20H02200, 21J14548).

Disclosures. The authors declare no conflicts of interest.

Data Availability. No data were generated or analyzed in the presented research.

REFERENCES

- R. H. Dennard, F. H. Gaensslen, V. L. Rideout, E. Bassous, and A. R. LeBlanc, "Design of ion-implanted MOSFET's with very small physical dimensions," *IEEE J. Solid-State Circuits* **9**, 256–268 (1974).
- P. Kapur, J. P. McVittie, and K. C. Saraswat, "Technology and reliability constrained future copper interconnects—Part I: resistance modeling," *IEEE Trans. Electron Devices* **49**, 590–597 (2002).
- P. Kapur, G. Chandra, J. P. McVittie, and K. C. Saraswat, "Technology and reliability constrained future copper interconnects—Part II: performance implications," *IEEE Trans. Electron Devices* **49**, 598–604 (2002).
- V. R. Almeida, C. A. Barrios, R. R. Panepucci, and M. Lipson, "All-optical control of light on a silicon chip," *Nature* **431**, 1081–1084 (2004).
- K. Ohashi, K. Nishi, and T. Shimizu, *et al.*, "On-chip optical interconnect," *Proc. IEEE* **97**, 1186–1198 (2009).
- M. Notomi, A. Shinya, K. Nozaki, T. Tanabe, S. Matsuo, E. Kuramochi, T. Sato, H. Taniyama, and H. Sumikara, "Low-power nanophotonic devices based on photonic crystals towards dense photonic network on chip," *IET Circuits Devices Syst.* **5**, 84–93 (2011).
- D. A. Miller, "Device requirements for optical interconnects to silicon chips," *Proc. IEEE* **97**, 1166–1185 (2009).
- S. Imai, K. Takaki, S. Kamiya, H. Shimizu, J. Yoshida, Y. Kawakita, T. Takagi, K. Hiraiwa, H. Shimizu, T. Suzuki, N. Iwai, T. Ishikawa, N. Tsukiji, and A. Kasukawa, "Recorded low power dissipation in highly reliable 1060-nm VCSELs for 'Green' optical interconnection," *IEEE J. Sel. Top. Quantum Electron.* **17**, 1614–1620 (2011).
- A. Kasukawa, "VCSEL technology for green optical interconnects," *IEEE Photon. J.* **4**, 642–646 (2012).
- P. Moser, J. Lott, P. Wolf, G. Larisch, H. Li, N. Ledentsov, and D. Bimberg, "56 fJ dissipated energy per bit of oxide-confined 850 nm VCSELs operating at 25 Gbit/s," *Electron. Lett.* **48**, 1292–1294 (2012).
- G. Larisch, S. Tian, and D. Bimberg, "Optimization of VCSEL photon lifetime for minimum energy consumption at varying bit rates," *Opt. Express* **28**, 18931–18937 (2020).
- M. Fujita, R. Ushigome, and T. Baba, "Continuous wave lasing in GaInAsP microdisk injection laser with threshold current of 40 μA ," *Electron. Lett.* **36**, 790–791 (2000).
- T. Carmon, L. Yang, and K. Vahala, "Dynamical thermal behavior and thermal self-stability of microcavities," *Opt. Express* **12**, 4742–4750 (2004).
- A. M. Armani and K. J. Vahala, "Heavy water detection using ultra-high-Q microcavities," *Opt. Lett.* **31**, 1896–1898 (2006).
- A. Elbaz, R. Arefin, and E. Sakat, *et al.*, "Reduced lasing thresholds in GeSn Microdisk cavities with defect management of the optically active region," *ACS Photon.* **7**, 2713–2722 (2020).
- H.-G. Park, S.-H. Kim, S.-H. Kwon, Y.-G. Ju, J.-K. Yang, J.-H. Baek, S.-B. Kim, and Y.-H. Lee, "Electrically driven single-cell photonic crystal laser," *Science* **305**, 1444–1447 (2004).
- D. Ohnishi, T. Okano, M. Imada, and S. Noda, "Room temperature continuous wave operation of a surface-emitting two-dimensional photonic crystal diode laser," *Opt. Express* **12**, 1562–1568 (2004).
- S. Matsuo, A. Shinya, T. Kakitsuka, K. Nozaki, T. Segawa, T. Sato, Y. Kawaguchi, and M. Notomi, "High-speed ultracompact buried heterostructure photonic-crystal laser with 13 fJ of energy consumed per bit transmitted," *Nat. Photonics* **4**, 648–654 (2010).
- S. Matsuo, K. Takeda, T. Sato, M. Notomi, A. Shinya, K. Nozaki, H. Taniyama, K. Hasebe, and T. Kakitsuka, "Room-temperature continuous-wave operation of lateral current injection wavelength-scale embedded active-region photonic-crystal laser," *Opt. Express* **20**, 3773–3780 (2012).
- K. Takeda, T. Sato, A. Shinya, K. Nozaki, W. Kobayashi, H. Taniyama, M. Notomi, K. Hasebe, T. Kakitsuka, and S. Matsuo, "Few-fJ/bit data transmissions using directly modulated lambda-scale embedded active region photonic-crystal lasers," *Nat. Photonics* **7**, 569–575 (2013).

21. E. Kuramochi, H. Duprez, J. Kim, M. Takiguchi, K. Takeda, T. Fujii, K. Nozaki, A. Shinya, H. Sumikura, H. Taniyama, S. Matsuo, and M. Notomi, "Room temperature continuous-wave nanolaser diode utilized by ultrahigh-Q few-cell photonic crystal nanocavities," *Opt. Express* **26**, 26598–26617 (2018).
22. S. Sakamoto, H. Naitoh, M. Ohtake, Y. Nishimoto, S. Tamura, T. Maruyama, N. Nishiyama, and S. Arai, "Strongly index-coupled membrane BH-DFB lasers with surface corrugation grating," *IEEE J. Sel. Top. Quantum Electron.* **13**, 1135–1141 (2007).
23. S. Arai, N. Nishiyama, T. Maruyama, and T. Okumura, "GaInAsP/InP membrane lasers for optical interconnects," *IEEE J. Sel. Top. Quantum Electron.* **17**, 1381–1389 (2011).
24. D. Inoue, J. Lee, T. Hiratani, Y. Atsui, T. Amemiya, N. Nishiyama, and S. Arai, "Sub-milliamper threshold operation of butt-jointed built-in membrane DFB laser bonded on Si substrate," *Opt. Express* **23**, 7771–7778 (2015).
25. T. Hiratani, D. Inoue, T. Tomiyasu, Y. Atsui, K. Fukuda, T. Amemiya, N. Nishiyama, and S. Arai, "Room-temperature continuous-wave operation of membrane distributed-reflector laser," *Appl. Phys. Express* **8**, 112701 (2015).
26. T. Tomiyasu, D. Inoue, T. Hiratani, K. Fukuda, N. Nakamura, T. Uryu, T. Amemiya, N. Nishiyama, and S. Arai, "20-Gbit/s direct modulation of GaInAsP/InP membrane distributed-reflector laser with energy cost of less than 100 fJ/bit," *Appl. Phys. Express* **11**, 012704 (2017).
27. Y. Jiao, N. Nishiyama, J. Tol, J. Engelen, V. Pogoretskiy, S. Reniers, A. Kashi, Y. Wang, V. Calzadilla, M. Spiegelberg, Z. Cao, K. Williams, T. Amemiya, and S. Arai, "InP membrane integrated photonics research," *Semicond. Sci. Technol.* **36**, 013001 (2020).
28. S. Yamaoka, N. Diamantopoulos, H. Nishi, R. Nakao, T. Fujii, K. Takeda, T. Hiraki, T. Tsurugaya, S. Kanazawa, H. Tanobe, T. Kakitsuka, T. Tsuchizawa, F. Koyama, and S. Matsuo, "Directly modulated membrane lasers with 108 GHz bandwidth on a high-thermal-conductivity silicon carbide substrate," *Nat. Photonics* **15**, 28–35 (2021).
29. T. Hiratani, D. Inoue, T. Tomiyasu, K. Fukuda, T. Amemiya, N. Nishiyama, and S. Arai, "High efficiency operation of membrane distributed-reflector lasers on silicon substrate," *IEEE J. Sel. Top. Quantum Electron.* **23**, 3700108 (2017).